

Ferroelectrically Switchable Half-Quantized Hall Effect

M. U. Muzaffar,^{§,†} Kai-Zhi Bai,[‡] Wei Qin,[¶] Guohua Cao,^{§,†} Bo Fu,[#] Ping Cui,^{§,†,*} Shun-Qing Shen,^{‡,*} and Zhenyu Zhang^{§,†,*}

[§]*International Center for Quantum Design of Functional Materials (ICQD), Hefei National Research Center for Physical Sciences at the Microscale, University of Science and Technology of China, Hefei, Anhui 230026, China*

[†]*Hefei National Laboratory, University of Science and Technology of China, Hefei, Anhui 230088, China*

[‡]*Department of Physics, The University of Hong Kong, China*

[¶]*Department of Physics, University of Science and Technology of China, Hefei, Anhui 230026, China*

[#]*School of Sciences, Great Bay University, Dongguan, Guangdong 523000, China*

*E-mail: cuipeg@ustc.edu.cn; sshen@hku.hk; zhangzy@ustc.edu.cn

ABSTRACT

Integrating ferroelectricity, antiferromagnetism, and topological quantum transport within a single material is rare, but crucial for developing next-generation quantum devices. Here, we propose a multiferroic heterostructure consisting of an antiferromagnetic MnBi_2Te_4 bilayer and an Sb_2Te_3 film is able to harbor the half-quantized Hall (HQH) effect with a ferroelectrically switchable Hall conductivity of $\pm e^2/2h$. We first show that, in the energetically stable configuration, the antiferromagnetic MnBi_2Te_4 bilayer opens a gap in the top surface bands of Sb_2Te_3 through proximity effect, while its bottom surface bands remain gapless; consequently, HQH conductivity of $e^2/2h$ can be sustained clockwise or counterclockwise depending on antiferromagnetic configuration of the MnBi_2Te_4 . Remarkably, when applying interlayer sliding within the MnBi_2Te_4 bilayer, its electric polarization direction associated with parity-time reversal symmetry breaking is reversed, accompanied by a reversal of the HQH conductivity. The proposed approach offers a powerful route to control topological quantum transport in antiferromagnetic materials by ferroelectricity.

Over the past decades, there have been rapid developments in two important areas of condensed matter physics, namely, quantum anomalous Hall effects¹⁻⁵ and ferroelectricity⁶⁻⁹, wherein symmetry breaking plays an integral part in the emergence of different quantum states¹⁰. The former, a fundamental transport phenomenon characterized by either integer^{2,3,11-14} or half-integer¹⁵⁻²⁰ quantum Hall conductance in multiples of e^2/h (where e is the electron charge and h is Planck's constant), arises from time-reversal symmetry (\hat{T}) breaking, while the latter results from inversion symmetry (\hat{P}) breaking, leading to spontaneous polarization²¹. Notably, unlike the integer quantum anomalous Hall effect in insulating phases, semi-magnetic topological insulators with a single gapless Dirac cone exhibit a half-integer quantized Hall conductivity, accompanied by a non-zero longitudinal resistance¹⁶. Recently, the broken \hat{P} symmetry in ferroelectric topological insulators has been actively explored, as it combines switchable polarization with robust topological surface states²²⁻²⁵, opening new avenues for designing innovative functional devices. The simultaneous breaking of both \hat{T} and \hat{P} symmetries may lead to even more exotic phenomena than breaking either \hat{T} or \hat{P} symmetry alone²⁶. In particular, ferroelectrically switchable and topologically protected edge states in a quantum regime may pave the way for developing next-generation quantum devices with high fault tolerance²⁷.

Recently, MnBi_2Te_4 has attracted significant attention as an intrinsic magnetic topological insulator with antiferromagnetic interlayer coupling, where the spins of the magnetic elements are ferromagnetically aligned within the ab plane²⁸⁻³¹. Consequently, the total magnetization depends on the film thickness, with films containing odd numbers of layers exhibiting the integer quantum anomalous Hall state³², while those containing even number of layers exhibiting zero net magnetization and no anomalous Hall conductivity³³. Here, the existence or absence of the quantum anomalous Hall effect can again be simply formulated based on symmetry arguments. Such a symmetry approach has recently led to the discovery of an asymmetric Hall response in the even layers of MnBi_2Te_4 , driven by $\hat{P}\hat{T}$ symmetry breaking through external electric fields³⁴ or by intrinsic ferroelectricity via layertronic sliding³⁵, countering the conventional wisdom that the anomalous Hall effect is tied to net magnetization. In particular, the demonstration of the electrical switching ability of the Hall conductance is not only a rare achievement due to conflicting symmetry requirements but also holds great promise for next-generation high-performance antiferromagnetic spintronic devices. However, to fully realize the application potentials, it is crucial to go beyond the existing paradigm that

primarily focuses on insulating phases by exploring alternative routes to achieve nonvolatile switching of the quantized Hall conductivity.

In this Letter, by going beyond the existing recipe in ferromagnetic systems^{16,36}, we propose a multiferroic MnBi₂Te₄/Sb₂Te₃ heterostructure with both antiferromagnetic and ferroelectric orders as an ideal platform for realizing the half-quantized Hall (HQH) conductivity with versatile tunability. We first show that, in the energetically stable configuration, the antiferromagnetic MnBi₂Te₄ bilayer opens a gap in the top surface bands of Sb₂Te₃ through proximity effect, while its bottom surface bands remain gapless; consequently, a HQH conductivity of $e^2/2h$ can be sustained clockwise or counterclockwise depending on the initial antiferromagnetic configuration of the MnBi₂Te₄ bilayer. More strikingly, when applying a relative interlayer sliding within the MnBi₂Te₄ bilayer, its electric polarization direction associated with the $\hat{P}\hat{T}$ symmetry breaking is reversed, accompanied by a reversal of the HQH conductivity as well. The proposed approach offers a powerful route to control topological quantum transport in antiferromagnetic materials by ferroelectricity, with appealing technological potentials.

First-principles calculations were performed using the projector-augmented wave method³⁷, implemented in the VASP code³⁸. The Perdew-Burke-Ernzerhof approximation was used to describe the exchange-correlation functional³⁹. To treat the localized $3d$ orbitals of Mn atoms in our proposed heterostructure, the (GGA)+ U method⁴⁰ was employed, with the $U_{eff} = 4.0$ eV, as suggested in Ref.⁴¹. Anomalous Hall conductivity was calculated using the WannierTools package⁴² in conjunction with the Wannier90⁴³. More computational details, along with the relevant references³⁷⁻⁵⁰, are given in the Supporting Information.

Tetradymite-type MnBi₂Te₄ forms a rhombohedral layered structure, similar to typical three-dimensional topological insulators (TIs) such as Bi₂Te₃, and belongs to the R3m space group (No. 166)²⁹. Its basic building block is a septuple layer (SL), stacked in the sequence Te-Bi-Te-Mn-Te-Bi-Te (see Figure 1(a)). Within each SL, a long-range ferromagnetic is established, while adjacent SLs exhibit antiferromagnetic coupling, with a Néel temperature (T_N) of 24 K⁵¹. Due to the inherent $\hat{P}\hat{T}$ symmetry, a film with an even number of layers of MnBi₂Te₄ in an antiferromagnetic order is centrosymmetric. However, breaking space inversion symmetry could potentially lead to the emergence of ferroelectricity⁷⁻⁹. In doing so, we first consider anti-AA stacking of an isolated MnBi₂Te₄ bilayer by rotating the top layer 180° relative to the bottom layer to break the inversion symmetry of the system, as shown in Figure S1. Such a stacking has been demonstrated in various hexagonal 2D materials, including

MnBi_2Te_4 ^{7, 8, 35, 50, 52}. Moreover, by further performing a lateral interlayer translation operation on the top layer of the anti-AA stacking with $\pm t_{\parallel}$ (where $t_{\parallel} = [1/3, -1/3]$ in fractional coordinates, as shown in Figure S1), two additional stacking configurations, namely anti-AB and anti-AC, can be obtained. Such inversion symmetry-broken configurations are energetically stable, while the anti-AA configuration is metastable due to the proximity of Te atoms across the interface³⁵. We then stack anti-AB and anti-AC configurations of MnBi_2Te_4 bilayers on thick Sb_2Te_3 to form semi-magnetic TIs, as shown in Figure 1(a). Our total energy calculations reveal that both the anti-AB and anti-AC based heterostructures are energetically nearly degenerate, exhibiting a camel-back feature in the total energy between the two states (see Figure 1(b)) that potentially signifies the emergence of ferroelectricity. The calculated binding energy for the anti-AB heterostructure is $-27.01 \text{ meV}/\text{\AA}^2$, comparable to that of typical vdW heterostructures⁵³. Here, the binding energy is defined as $E_b = E_{\text{total}} - E_{\text{MBT}} - E_{\text{ST}}$, with E_{total} , E_{MBT} , and E_{ST} being the total energies of the heterostructure, freestanding bilayer MnBi_2Te_4 , and freestanding five quintuple layers (QLs) of Sb_2Te_3 , respectively.

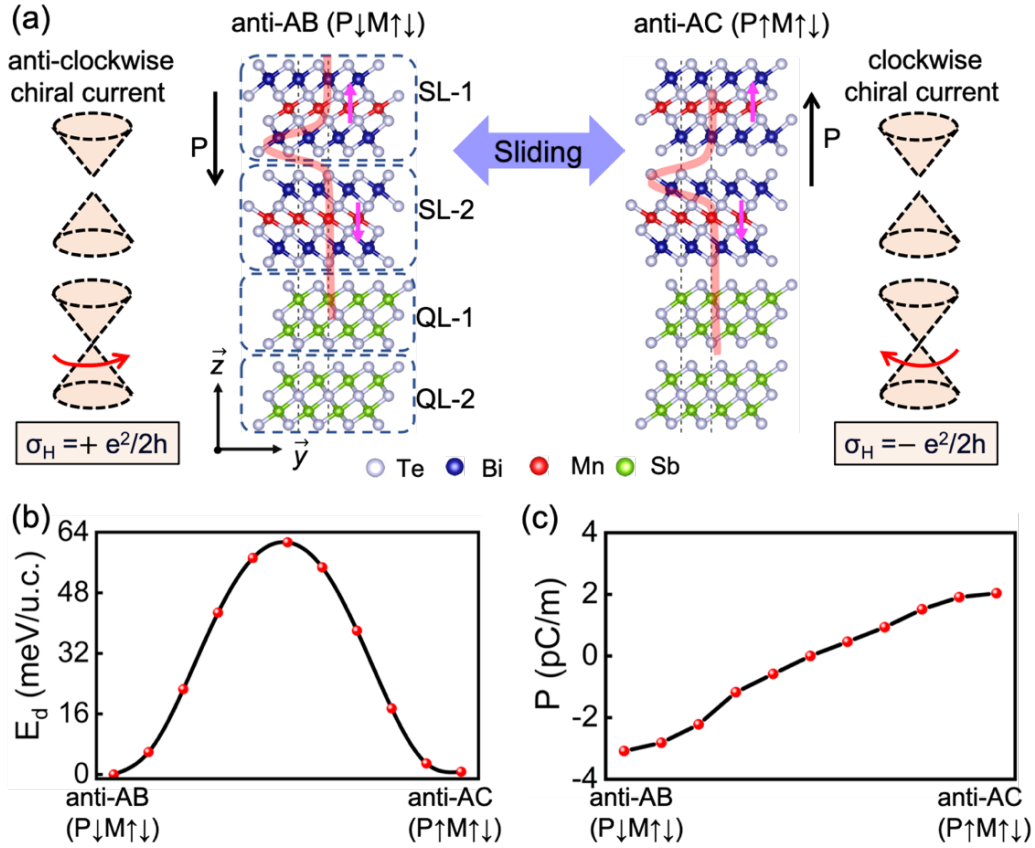


Figure 1. (a) Atomic structures of the two switchable ferroelectric states in the $\text{MnBi}_2\text{Te}_4/\text{Sb}_2\text{Te}_3$ heterostructure, along with the ferroelectric switching mechanism. In the

two central columns, a schematic illustration is shown between the density distribution of the gapped surface states (as represented by the red lines within the crystals) and the tunability of the parity anomaly of the gapless Dirac cone at the bottom surface. The Mn 3*d* atoms are labeled in red, with opposite spin directions indicated by the magenta arrows and opposite polarizations shown by the black arrows. (b) Energy profile and (c) variation in the out-of-plane electric polarization during the ferroelectric switching of the MnBi₂Te₄/Sb₂Te₃ heterostructure.

Next, to quantify the spontaneous polarizations (P) in the two stacking heterostructures, we employ the Berry phase approach⁵⁴ and the ferroelectric switching pathway is determined via the nudged elastic band (NEB) method⁵⁵. We find that the anti-AB and anti-AC heterostructures exhibit relatively high P values of -3.08 pC/m and 2.03 pC/m, respectively, and the energy barrier between them is 61 meV per unit cell (u.c.) (see Figure 1(b)). This barrier is higher than that of isolated MnBi₂Te₄ bilayers (31 meV/u.c.) but still lower than or comparable to that of well-established 2D ferroelectric materials such as In₂Se₃ (66 meV/u.c.)⁵⁶. Thus, MnBi₂Te₄/Sb₂Te₃ semi-magnetic TI exhibits robust ferroelectricity with switchable out-of-plane polarization, making it ideal for low-energy, non-volatile switching and memory devices.

Now we discuss the magnetic properties during ferroelectric polarization reversal due to magnetoelectric coupling in the MnBi₂Te₄/Sb₂Te₃ heterostructure. As shown in Figure 1(b,c) and Figure S2, all the stacking configurations of the MnBi₂Te₄/Sb₂Te₃ heterostructure along the kinetic pathway prefer out-of-plane antiferromagnetic ground state. Moreover, compared to the freestanding MnBi₂Te₄ bilayer (0.24 meV per Mn atom), the MnBi₂Te₄/Sb₂Te₃ heterostructure exhibits enhanced magnetic anisotropy, increasing to 0.33 meV and 0.39 meV per Mn atom for the anti-AB and anti-AC stackings, respectively. Typically, the magnetic ordering temperature of a material is closely related to its magnetic anisotropy, with a higher anisotropy leading to higher Curie or Néel temperature⁵⁷. To confirm this conjecture, we have performed Monte Carlo simulations to estimate T_N for the anti-AB (P↓M↑↓) configuration of the MnBi₂Te₄/Sb₂Te₃ heterostructure as a specific example (for details, see Section S1). Using the DFT-derived exchange interactions J and magnetic anisotropy energy (E_{MAE}), the estimated T_N for the anti-AB (P↓M↑↓) configuration is 38.7 K (see Figure S3), which is higher than that of an isolated MnBi₂Te₄ bilayer, given by 24 K⁵⁸.

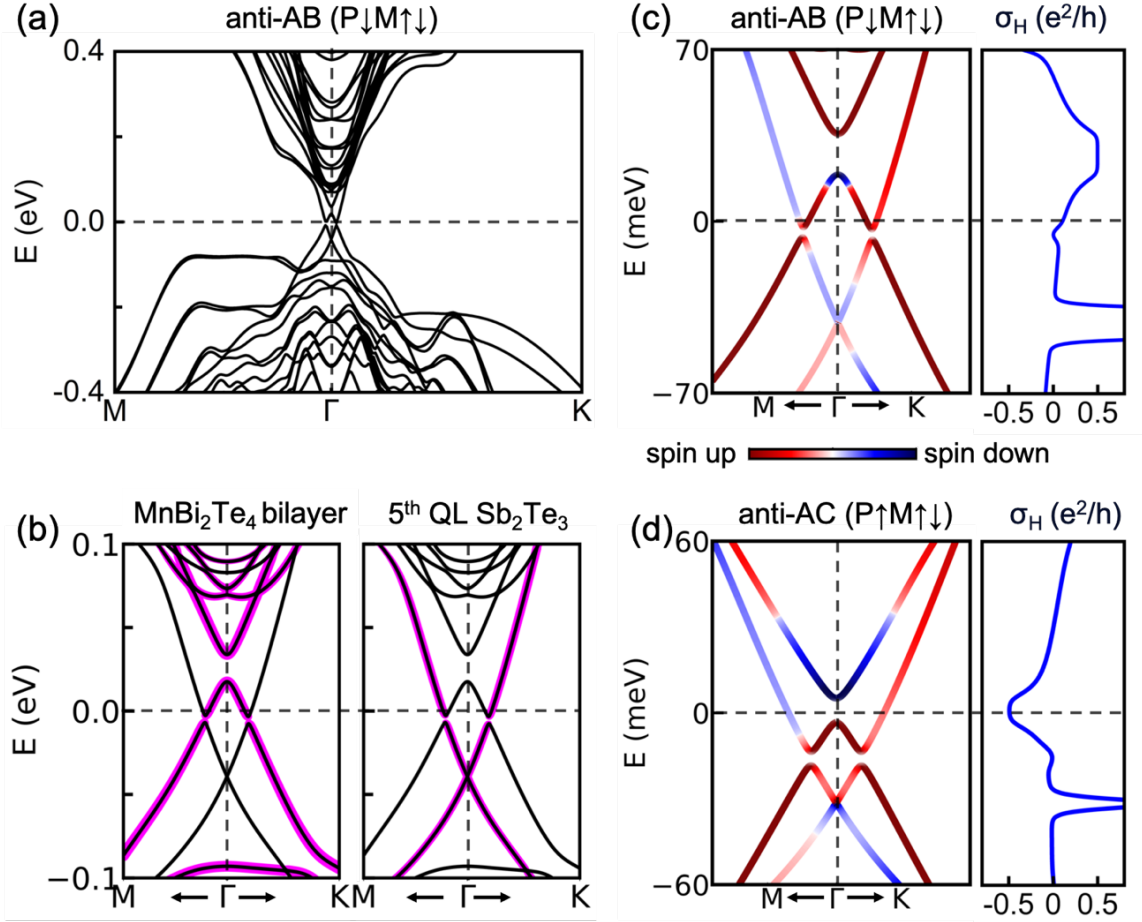


Figure 2. (a) Electronic structure and (b) zoomed-in views of the constituent band structures for the anti-AB ($P\downarrow M\uparrow\downarrow$) configuration of the $\text{MnBi}_2\text{Te}_4/\text{Sb}_2\text{Te}_3$ heterostructure. (c,d) Electronic structures (left panels) and HQH conductivities (right panels) as functions of energy for the two ferroelectrically switchable states of the $\text{MnBi}_2\text{Te}_4/\text{Sb}_2\text{Te}_3$ heterostructure, with the projected expectation value of the spin operator S_z also indicated by the spin bar.

Next, we turn our attention to the electronic structure and quantum transport properties of the two switchable states of the $\text{MnBi}_2\text{Te}_4/\text{Sb}_2\text{Te}_3$ heterostructure. The Sb_2Te_3 film possesses two gapless surface Dirac cones, and their mutual coupling is critically dependent on the film thickness⁵⁹. To crosscheck that the 5-QL film of Sb_2Te_3 is thick enough, we project the wave functions of the topmost or bottommost QL onto the band structure, as shown in Figure S4. We see that the topologically nontrivial surface states cross the Fermi level, indicating sufficient film thickness to decouple the top and bottom surface states. Upon depositing the bilayer MnBi_2Te_4 on top of Sb_2Te_3 , the exchange interaction between the surface electrons of

the TI and magnetic elements in the MnBi_2Te_4 induces an energy gap (Δ) in the top-surface Dirac cone of the TI while the bottom surface Dirac cone remain gapless, as shown in Figure 2(a,b). To distinguish between the two switchable states of anti-AB ($\text{P}\downarrow\text{M}\uparrow\downarrow$) and anti-AC ($\text{P}\uparrow\text{M}\uparrow\downarrow$), we calculate the spin-dependent band structures with spin-orbit coupling, as shown in Figure 2 (c,d). Remarkably, both configurations exhibit a spin-dependent magnetic gap around the Γ point, which varies upon reversing the direction of the electric polarization. Furthermore, as the proposed heterostructure also exhibits net antiferromagnetic order, when the directions of the magnetic moments are flipped while keeping the polarization direction fixed, the sign of the magnetic gap changes as well, as shown in Figure S5. Such a spin-dependent magnetic gap can serve as a control parameter for the anomalous Hall conductivity, as confirmed later. The calculated magnetic gap for the anti-AB ($\text{P}\downarrow\text{M}\uparrow\downarrow$) and anti-AC ($\text{P}\uparrow\text{M}\uparrow\downarrow$) configurations is 16.2 meV and 8.4 meV, respectively, and these values are tunable through strain engineering, as also demonstrated for the anti-AB ($\text{P}\downarrow\text{M}\uparrow\downarrow$) configuration as an example (see Figure S6). Here it is noted that due to quantum confinement effect, a tiny gap appears below the Fermi level, and it decreases with the thicker Sb_2Te_3 layers; however, due to computational constraints, we restrict the analysis to up to 5-QLs.

The Hall conductivity at zero temperature can be calculated using the Kubo formula⁶⁰,

$$\sigma_H = -\frac{e^2}{h} \int_{BZ} \frac{dk_x dk_y}{2\pi} \Omega^z(k_x, k_y). \quad (1)$$

Here the Berry curvature is defined as

$$\Omega^z(k_x, k_y) = -2 \text{Im} \sum_n^{\text{occupied}} \sum_{n'}^{\text{empty}} \frac{\langle \Psi_{nk} | \hbar v_x | \Psi_{n'k} \rangle \langle \Psi_{n'k} | \hbar v_y | \Psi_{nk} \rangle}{(\varepsilon_{nk} - \varepsilon_{n'k})^2}, \quad (2)$$

where Ψ_{nk} is the Bloch wave function with eigenvalues ε_{nk} and v_x (v_y) is the velocity operator along the x (y) direction. The calculated Hall conductivities for the two switchable ferroelectric states of the $\text{MnBi}_2\text{Te}_4/\text{Sb}_2\text{Te}_3$ heterostructure are plotted in Figure 2(c,d) where both configurations exhibit the HQH effect with a Hall conductance of magnitude $e^2/2h$ within the magnetic gap. In sharp contrast, an isolated MnBi_2Te_4 bilayer is a trivial insulator with zero Hall conductivity due to its inherent $\hat{P}\hat{T}$ symmetry (see Figure S9). The switchable HQH conductivity can be explained based on Berry curvature analyses, as presented in Figure 3. It can be seen that reversing the polarization direction from the anti-AC ($\text{P}\uparrow\text{M}\uparrow\downarrow$) to the anti-AB ($\text{P}\downarrow\text{M}\uparrow\downarrow$) state while keeping the magnetic moment directions fixed changes the sign of the

Berry curvature around the Γ point, leading to a switchable Hall conductivity from $-e^2/2h$ to $+e^2/2h$. This controllable switching of the Berry curvature and the corresponding QH conductivity through electric field is not only experimentally feasible³⁴ but also highly desirable for device applications. These analyses show that switchable polarization and/or magnetization can be used as control parameters for realizing and manipulating the QH effect.

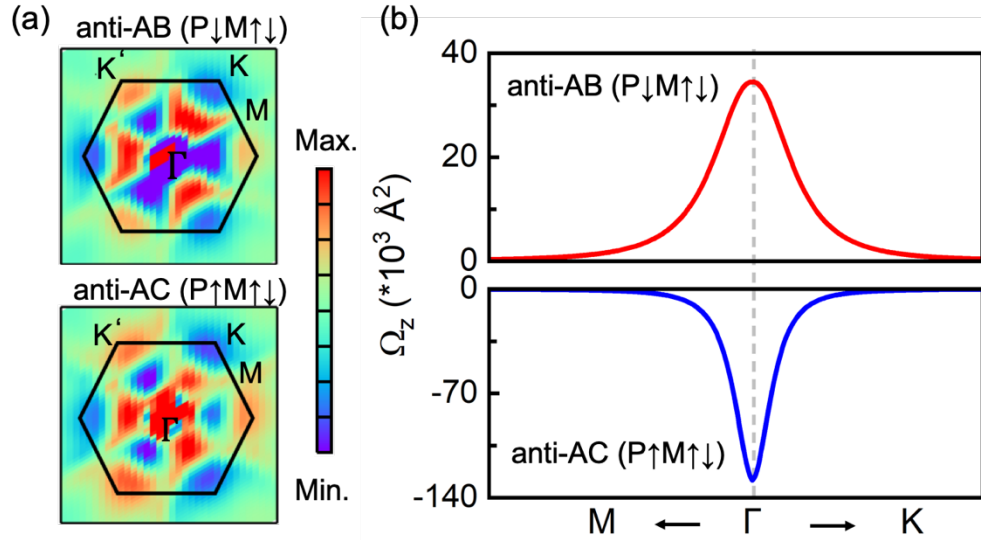


Figure 3. (a) Berry curvature distributions in the 2D Brillouin zone, and (b) along high-symmetry points, for the two ferroelectrically switchable states of the $\text{MnBi}_2\text{Te}_4/\text{Sb}_2\text{Te}_3$ heterostructure.

It is worth noting that, to realize QH conductivity, an antiferromagnetic MnBi_2Te_4 bilayer serves as a prototypical example to open the energy gap in the top surface bands of Sb_2Te_3 , while keeping the bottom surface bands gapless. This proposed approach for realizing QH conductivity is conceptually generic and applicable to other related 2D semi-magnetic TIs composed of antiferromagnetic–nonmagnetic topological material combinations, provided the magnetization is strong enough to induce an energy gap in the top-surface bands of the TI while keeping the bottom-surface bands gapless (for details, see Section S3). As for MnBi_2Te_4 , it typically exhibits intrinsic antisite defects that may influence the energy gap in the top-surface bands of TI,⁶¹ and several effective methods^{51,62}, such as slower cooling and additional thermal annealing, are commonly employed to drive the system towards thermodynamic equilibrium during growth and promote the formation of high-quality, uniform single crystals.

In Figure 4(a,b), we present the real-space charge density distributions of the upper-surface topological surface states at the Γ point for both the anti-AB ($P\downarrow M\uparrow\downarrow$) and anti-AC ($P\uparrow M\uparrow\downarrow$) configurations of the $\text{MnBi}_2\text{Te}_4/\text{Sb}_2\text{Te}_3$ heterostructure. It can be seen that a large peak in the real-space charge density distribution primarily appears in the bottom layer of MnBi_2Te_4 for the anti-AC ($P\uparrow M\uparrow\downarrow$) configuration, namely, the MnBi_2Te_4 layer in proximity to the TI film. Upon reversing the polarization, the topological surface states of the TI in proximity with the MnBi_2Te_4 float up towards the top MnBi_2Te_4 layer. This floating behavior of the surface states leads to a strong interaction with the magnetism, resulting in a larger surface band gap observed in the anti-AB ($P\downarrow M\uparrow\downarrow$) configuration compared to the anti-AC ($P\uparrow M\uparrow\downarrow$).

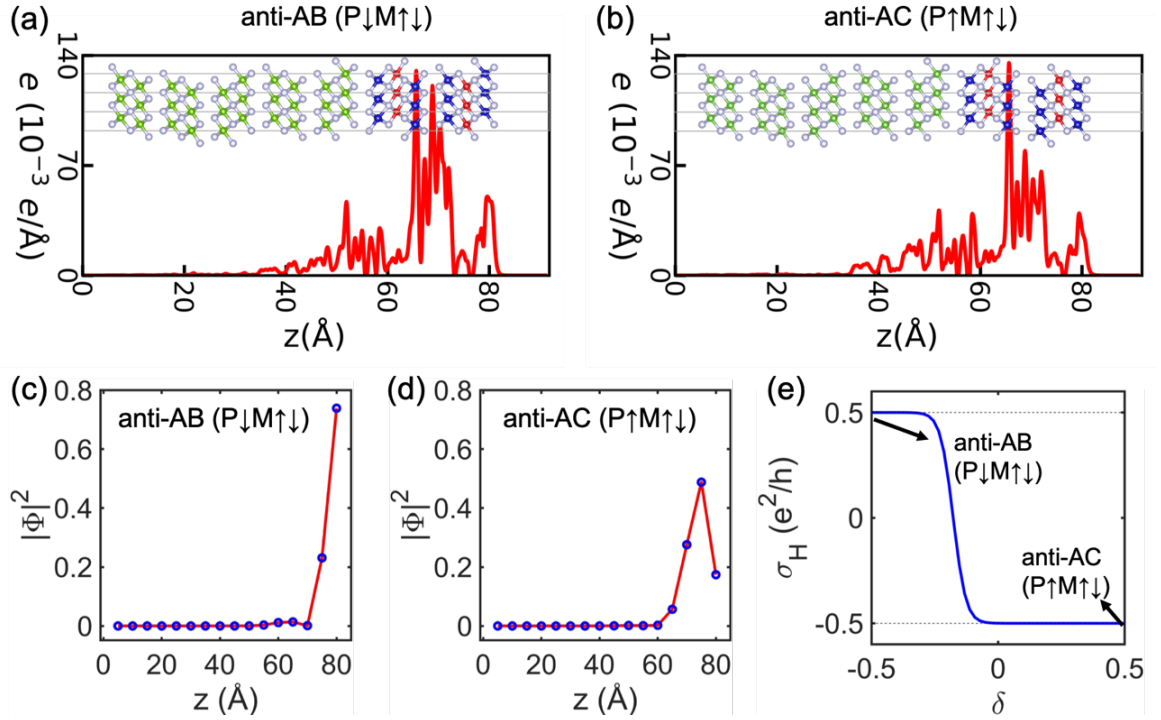


Figure 4. (a,b) Electron density distributions of the gapped topological surface states at the Γ point for both polarizations, with the crystal structures shown in the insets. (c,d) Density distributions of the gapped surface states for both ferroelectric states and (e) HQH conductivity as a function of inter-layer coupling strength (δ).

Going beyond first principles calculations, we employ a tight-binding lattice model to explore the impact of inter-layer coupling strength (δ) on the Hall conductivity in our proposed heterostructure (for details, see Section S2). In Figure 4(c-e), we present the calculated density distributions of the surface states and the Hall conductivity as a function of δ , revealing a

quantum phase transition characterized by a switchable Hall conductivity of $\pm e^2/2h$. This quantum phase transition can be understood as the peak of the surface state density in the anti-AB ($P\downarrow M\uparrow\downarrow$) configuration is localized at the first MnBi_2Te_4 layer; while in the anti-AC ($P\uparrow M\uparrow\downarrow$) configuration, the peak shifts to the second MnBi_2Te_4 layer, consistent with our first-principles results. The sign of the magnetic gap is correlated with the parity anomaly of the gapless Dirac cone at the bottom surface of the TI film, which determines the sign of its half-quantized Hall conductivity. These analyses suggest that the switching of ferroelectricity alters the dominance of density distribution within the MnBi_2Te_4 layers, leading to switchable Hall conductivity in the $\text{MnBi}_2\text{Te}_4/\text{Sb}_2\text{Te}_3$ semi-magnetic TI.

Before closing, we wish to emphasize the significance of this work from both the fundamental and practical aspects. First, our work explores the delicate interplay between the surface states of a TI and antiferromagnetism, uncovering a pathway to achieve QH conductance that challenges the prevailing notion that antiferromagnetic systems with zero net magnetization yield no anomalous Hall effect. More importantly, the switching ability of the QH conductance via ferroelectricity in the proposed semi-magnetic $\text{MnBi}_2\text{Te}_4/\text{Sb}_2\text{Te}_3$ heterostructure can significantly broaden the scope of practical device applications, especially compared to systems that rely on ferromagnetic phase^{3, 15, 16, 32, 35}. Secondly, since observation temperatures of the quantum anomalous Hall effect have so far been limited to only a few kelvin^{3, 32, 63, 64}, significant efforts continue to be made to identify new quantum topological materials in the antiferromagnetic phase^{65, 66}. Here, the proposed antiferromagnetic phase exhibits a large magnetic gap of 16.47 meV and a relatively higher Néel temperature of ~ 39 K suggesting that the observation temperature for the QH effect in the present system can be much higher than what has been observed so far in the ferromagnetic phase (~ 1 K)¹⁶. From the practical aspect, the proposed $\text{MnBi}_2\text{Te}_4/\text{Sb}_2\text{Te}_3$ heterostructure is also physically realistic. Moreover, our detailed *ab initio* molecular dynamics simulations have shown that the predicted heterostructure is stable at least up to 200 K (see Figure S10), thereby offering a desirable temperature range for the fabrication of such systems and exploration of the emergent quantum transport properties.

In summary, following the structural and compositional compatibility between MnBi_2Te_4 and Sb_2Te_3 , we have comprehensively demonstrated that the proposed multiferroic $\text{MnBi}_2\text{Te}_4/\text{Sb}_2\text{Te}_3$ heterostructures exhibit moderate sliding energy barriers and ferroelectrically switchable QH conductivity at elevated temperatures. This central finding

offers a highly viable route for designing low-power memory devices with antiferromagnetic spintronic applications at relatively high temperatures.

ACKNOWLEDGEMENTS

This work was supported by the National Natural Science Foundation of China (Grant Nos., 12374458, 12488101, 11974323, 12004368, 12474134, W2433002 and GG9990001216), the Innovation Program for Quantum Science and Technology (Grant No. 2021ZD0302800), the Strategic Priority Research Program of Chinese Academy of Sciences (Grant No. XDB0510200), the Anhui Provincial Key Research and Development Project (Grant No. 2023z04020008), the Research Grants Council, University Grants Committee, Hong Kong (Grant Nos. C7012-21G and 17301823), and Quantum Science Center of Guangdong-Hong Kong-Macao Greater Bay Area (Grant No. GDZX2301005).

■ REFERENCES

- (1) F. D. M. Haldane. Model for a Quantum Hall effect without Landau Levels: Condensed-Matter Realization of the "Parity Anomaly", *Phys. Rev. Lett.* **1988**, 61, 2015.
- (2) Rui Yu; Wei Zhang; Hai-Jun Zhang, *et al.* Quantized anomalous Hall effect in magnetic topological insulators, *Science* **2010**, 329, 61-64.
- (3) Cui-Zu Chang; Jinsong Zhang; Xiao Feng, *et al.* Experimental observation of the Quantum anomalous Hall effect in a magnetic topological insulator, *Science* **2013**, 340, 167-170.
- (4) Naoto Nagaosa; Jairo Sinova; Shigeki Onoda, *et al.* Anomalous Hall Effect, *Rev. Mod. Phys.* **2010**, 82, 1539-1592.
- (5) Di Xiao; Ming-Che Chang; Qian Niu. Berry phase effects on electronic properties, *Rev. Mod. Phys.* **2010**, 82, 1959-2007.
- (6) Lei Li; Menghao Wu. Binary compound bilayer and multilayer with vertical polarizations: two-dimensional ferroelectrics, multiferroics, and nanogenerators, *ACS Nano* **2017**, 11, 6382-6388.
- (7) Kenji Yasuda; Xirui Wang; Kenji Watanabe, *et al.* Stacking-engineered ferroelectricity in bilayer boron nitride, *Science* **2021**, 372, 1458-1462.

- (8) M. Vizner Stern; Y. Waschitz; W. Cao, *et al.* Interfacial ferroelectricity by van der Waals sliding, *Science* **2021**, 372, 1462-1466.
- (9) Peng Meng; Yaze Wu; Renji Bian, *et al.* Sliding induced multiple polarization states in two-dimensional ferroelectrics, *Nat. Commun.* **2022**, 13, 7696.
- (10) LuoJun Du; Tawfique Hasan; Andres Castellanos-Gomez, *et al.* Engineering symmetry breaking in 2D layered materials, *Nat. Rev. Phys.* **2021**, 3, 193-206.
- (11) Zhenhua Qiao; Shengyuan A. Yang; Wanxiang Feng, *et al.* Quantum anomalous Hall effect in graphene from Rashba and exchange effects, *Phys. Rev. B* **2010**, 82, 161414(R).
- (12) Wang-Kong Tse; Zhenhua Qiao; Yugui Yao, *et al.* Quantum anomalous Hall effect in single-layer and bilayer graphene, *Phys. Rev. B* **2011**, 83, 155447.
- (13) J. G. Checkelsky; R. Yoshimi; A. Tsukazaki, *et al.* Trajectory of the anomalous Hall effect towards the quantized state in a ferromagnetic topological insulator, *Nature Phys.* **2014**, 10, 731-736.
- (14) Zhiyong Wang; Chi Tang; Raymond Sachs, *et al.* Proximity-Induced Ferromagnetism in Graphene Revealed by the Anomalous Hall Effect, *Phys. Rev. Lett.* **2015**, 114, 016603.
- (15) Ruie Lu; Hongyi Sun; Shiv Kumar, *et al.* Half-magnetic topological insulator with magnetization-induced dirac gap at a selected surface, *Phys. Rev. X* **2021**, 11, 011039.
- (16) M. Mogi; Y. Okamura; M. Kawamura, *et al.* Experimental signature of the parity anomaly in a semi-magnetic topological insulator, *Nature Phys.* **2022**, 18, 390–394.
- (17) Bo Fu; Jin-Yu Zou; Zi-Ang Hu, *et al.* Quantum anomalous semimetals, *npj Quantum Mater.* **2022**, 7, 94.
- (18) Jin-Yu Zou; Rui Chen; Bo Fu, *et al.* Half-quantized Hall effect at the parity-invariant Fermi surface, *Phys. Rev. B* **2023**, 107, 125153.
- (19) Bo Fu; Kai-Zhi Bai; Shun-Qing Shen. Half-quantum mirror Hall effect, *Nat. Commun.* **2024**, 15, 6939.
- (20) Shun-Qing Shen. Half quantized Hall effect, *Coshare Science* **2024**, 02, 01.
- (21) W. P. Mason; B. T. Matthias. Theoretical model for explaining the ferroelectric effect in barium titanate, *Phy. Rev.* **1948**, 74, 1622.

- (22) Awadhesh Narayan. Class of Rashba ferroelectrics in hexagonal semiconductors, *Phy. Rev. B* **2015**, 92, 220101.
- (23) Shi Liu; Youngkuk Kim; Liang Z. Tan, *et al.* Strain-induced ferroelectric topological insulator, *Nano Lett.* **2016**, 16, 1663-1668.
- (24) Bartomeu Monserrat; Joseph W. Bennett; Karin M. Rabe, *et al.* Antiferroelectric topological insulators in orthorhombic AMgBi compounds (A= Li, Na, K), *Phy. Rev. Lett.* **2017**, 119, 036802.
- (25) Jun-Jie Zhang; Dongyang Zhu; Boris I. Yakobson. Heterobilayer with ferroelectric switching of topological state, *Nano Lett.* **2020**, 21, 785-790.
- (26) Shiqi Xia; Dimitrios Kaltsas; Daohong Song, *et al.* Nonlinear tuning of PT symmetry and non-Hermitian topological states, *Science* **2021**, 372, 72-76.
- (27) Louis Ponet; S. Artyukhin; Th. Kain, *et al.* Topologically protected magnetoelectric switching in a multiferroic, *Nature* **2022**, 607, 81-85.
- (28) Yan Gong; J. W. Guo; J. H. Li, *et al.* Experimental realization of an intrinsic magnetic topological insulator, *Chinese Phys. Lett.* **2019**, 36, 076801.
- (29) M. M. Otrokov; I. I. Klimovskikh; H. Bentmann, *et al.* Prediction and observation of an antiferromagnetic topological insulator, *Nature* **2019**, 576, 416-422.
- (30) Dongqin Zhang; Minji Shi; Tongshuai Zhu, *et al.* Topological axion states in the magnetic insulator MnBi₂Te₄ with the quantized magnetoelectric effect, *Phys. Rev. Lett.* **2019**, 122, 206401.
- (31) Jiaheng Li; Yang Li; Shiqiao Du, *et al.* Intrinsic magnetic topological insulators in van der Waals layered MnBi₂Te₄-family materials, *Sci. Adv.* **2019**, 5, eaaw5685.
- (32) Yujun Deng; Yijun Yu; Meng Zhu Shi, *et al.* Quantum anomalous Hall effect in intrinsic magnetic topological insulator MnBi₂Te₄, *Science* **2020**, 367, 895-900.
- (33) Chang Liu; Yongchao Wang; Hao Li, *et al.* Robust axion insulator and Chern insulator phases in a two-dimensional antiferromagnetic topological insulator, *Nat. Mater.* **2020**, 19, 522-527.
- (34) Anyuan Gao; Yu-Fei Liu; Chaowei Hu, *et al.* Layer Hall effect in a 2D topological axion antiferromagnet, *Nature* **2021**, 595, 521-525.

- (35) Tengfei Cao; Ding-Fu Shao; Kai Huang, *et al.* Switchable anomalous Hall effects in polar-stacked 2D antiferromagnet MnBi₂Te₄, *Nano Letters* **2023**, 23, 3781-3787.
- (36) Ryota Watanabe; Ryutaro Yoshimi; Kei S. Takahashi, *et al.* Gate-electric-field and magnetic-field control of versatile topological phases in a semi-magnetic topological insulator, *Appl. Phys. Lett.* **2023**, 123, 183102.
- (37) Blöchl, P. E. Projector augmented-wave method, *Phys. Rev. B* **1994**, 50, 17953.
- (38) G. Kresse; Furthmüller, J. Efficient iterative schemes for ab initio total-energy calculations using a plane-wave basis set, *Phys. Rev. B* **1996**, 54, 11169.
- (39) John P. Perdew; Kieron Burke; Matthias Ernzerhof. Generalized gradient approximation made simple, *Phys. Rev. Lett.* **1996**, 77, 3865.
- (40) A. I. Liechtenstein; V. I. Anisimov; Zaanen, J. Density-functional theory and strong interactions: Orbital ordering in Mott-Hubbard insulators, *Phys. Rev. B* **1995**, 52, R5467.
- (41) Huisheng Zhang; Wenjia Yang; Yingying Wang, *et al.* Tunable topological states in layered magnetic materials of MnSb₂Te₄, MnBi₂Se₄, and MnSb₂Se₄, *Phys. Rev. B* **2021**, 103, 094433.
- (42) QuanSheng Wu; ShengNan Zhang; Hai-Feng Song, *et al.* WannierTools: An open-source software package for novel topological materials, *Comput. Phys. Commun.* **2018**, 224, 405-416.
- (43) Arash A. Mostofi; Jonathan R. Yates; Young-Su Lee, *et al.* Wannier90: A tool for obtaining maximally-localised Wannier functions, *Comput. Phys. Commun.* **2008**, 178, 685-699.
- (44) Xuelai Li; Feng Rao; Zhitang Song, *et al.* Experimental and theoretical study of silicon-doped Sb₂Te₃ thin films: Structure and phase stability, *Appl. Surf. Sci.* **2011**, 257, 4566-4568.
- (45) Stefan Grimme; Jens Antony; Stephan Ehrlich, *et al.* A consistent and accurate ab initio parametrization of density functional dispersion correction (DFT-D) for the 94 elements H-Pu, *J. Chem. Phys.* **2010**, 132, 154104.
- (46) Shuichi Nosé. A unified formulation of the constant temperature molecular dynamics methods, *J. Chem. Phys.* **1984**, 81, 511-519.
- (47) Shun-Qing Shen, *Topological insulators*. Second ed.; Springer: Berlin, 2017; Vol. 187.

- (48) Haijun Zhang; Chao-Xing Liu; Xiao-Liang Qi, *et al.* Topological insulators in Bi₂Se₃, Bi₂Te₃ and Sb₂Te₃ with a single Dirac cone on the surface, *Nature Phys.* **2009**, 5, 438-442.
- (49) Xu He; Nicole Helbig; Matthieu J. Verstraete, *et al.* TB2J: A python package for computing magnetic interaction parameters, *Comput. Phys. Commun.* **2021**, 264, 107938.
- (50) Nikhil Sivadas; Satoshi Okamoto; Xiaodong Xu, *et al.* Stacking-dependent magnetism in bilayer CrI₃, *Nano Lett.* **2018**, 18, 7658-7664.
- (51) Alexander Zeugner; Frederik Nietschke; Anja U. B. Wolter, *et al.* Chemical aspects of the candidate antiferromagnetic topological insulator MnBi₂Te₄, *Chem. Mater.* **2019**, 31, 2795-2806.
- (52) Weijiong Chen; Zeyuan Sun; Zhongjie Wang, *et al.* Direct observation of van der Waals stacking-dependent interlayer magnetism, *Science* **2019**, 366, 983-987.
- (53) Ze Liu; Jefferson Zhe Liu; Yao Cheng, *et al.* Interlayer binding energy of graphite: A mesoscopic determination from deformation, *Phy. Rev. B* **2012**, 85, 205418.
- (54) R. D. King-Smith; David Vanderbilt. Theory of polarization of crystalline solids, *Phy. Rev. B* **1993**, 47, 1651.
- (55) G. Henkelman; B. P. Uberuaga; H. Jónsson. A climbing image nudged elastic band method for finding saddle points and minimum energy paths, *J. Chem. Phys.* **2000**, 113, 9901-9904.
- (56) Wenjun Ding; Jianbao Zhu; Zhe Wang, *et al.* Prediction of intrinsic two-dimensional ferroelectrics in In₂Se₃ and other III₂-VI₃ van der Waals materials, *Nat. Commun.* **2017**, 8, 14956.
- (57) Xue-Juan Dong; Jing-Yang You; Zhen Zhang, *et al.* Great enhancement of Curie temperature and magnetic anisotropy in two-dimensional van der Waals magnetic semiconductor heterostructures, *Phy. Rev. B* **2020**, 102, 144443.
- (58) M. M. Otrokov; I. P. Rusinov; M. Blanco-Rey, *et al.* Unique thickness-dependent properties of the van der Waals interlayer antiferromagnet MnBi₂Te₄ films, *Phys. Rev. Lett.* **2019**, 122, 107202.
- (59) Kyungwha Park; J. J. Heremans; V. W. Scarola, *et al.* Robustness of topologically protected surface states in layering of Bi₂Te₃ thin films, *Phys. Rev. Lett.* **2010**, 105, 186801.

- (60) Yugui Yao; Leonard Kleinman; A. H. MacDonald, *et al.* First principles calculation of anomalous Hall conductivity in ferromagnetic bcc Fe, *Phys. Rev. Lett.* **2004**, 92, 037204.
- (61) Xi Wu; Chao Ruan; Peizhe Tang, *et al.* Irremovable Mn-Bi Site Mixing in MnBi_2Te_4 , *Nano Lett.* **2023**, 23, 5048-5054.
- (62) Y. J. Chen; L. X. Xu; J. H. Li, *et al.* Topological electronic structure and its temperature evolution in antiferromagnetic topological insulator MnBi_2Te_4 , *Phy. Rev. X* **2019**, 9, 041040.
- (63) Guorui Chen; Aaron L Sharpe; Eli J Fox, *et al.* Tunable correlated Chern insulator and ferromagnetism in a moiré superlattice, *Nature* **2020**, 579, 56-61.
- (64) Tonghang Han; Zhengguang Lu; Yuxuan Yao, *et al.* Large quantum anomalous Hall effect in spin-orbit proximitized rhombohedral graphene, *Science* **2024**, 384, 647-651.
- (65) Jian Zhou; Qi-Feng Liang; Hongming Weng, *et al.* Predicted quantum topological Hall effect and noncoplanar antiferromagnetism in $\text{K}_{0.5}\text{RhO}_2$, *Phy. Rev. Lett.* **2016**, 116, 256601.
- (66) Zhenhua Qiao; Wei Ren; Hua Chen, *et al.* Quantum anomalous Hall effect in graphene proximity coupled to an antiferromagnetic insulator, *Phys. Rev. Lett.* **2014**, 112, 116404.